Chemical Engineering Journal 146 (2009) 194–204

Contents lists available at ScienceDirect

Chemical Engineering Journal

journal homepage: www.elsevier.com/locate/cej

Experimental and numerical modeling of the mass transfer between rock matrix and fracture

J.J. Trivedi, T. Babadagli *

University of Alberta, Department of Civil and Environmental Engineering, School of Mining and Petroleum, 3-112 Markin CNRL-NREF, Edmonton, AB, Canada T6G 2W2

ARTICLE INFO

Article history:
Received 11 June 2007
Received in revised form 16 May 2008
Accepted 23 May 2008

Keywords:
Mass transfer
Diffusion
Enhanced oil recovery
Greenhouse gas sequestration
Groundwater contamination
Fractured reservoirs
Finite elements
Matrix–fracture interaction

ABSTRACT

Mass transfer between matrix and fracture is encountered during enhanced oil recovery applications, greenhouse gas sequestration and contaminant transportation in naturally fractured subsurface reservoirs. We used a combination of laboratory scale physical experiments and numerical simulations to evaluate the mass transfer between fracture and matrix and effective diffusion/dispersion in the matrix of naturally fractured subsurface reservoirs. Experiments on artificially fractured porous media showed the influence of various factors such as injection flow rate, matrix–fracture length, solute viscosity and density and matrix porosity/permeability on solvent/solute diffusion into/from the porous matrix media from/into the adjacent fracture. Mass transfer between matrix and fracture was simulated using advection–convection equation governing the system. Experimental results were compared with the results from numerical simulations to evaluate the major contributing parameters, mass transfer rate and effective matrix diffusion coefficient. It was found that effective matrix diffusion coefficient in the matrix is higher than the mutual diffusion coefficient. The mass transfer rate was found to be linearly dependent on velocity and affected by wettability as well as rock properties. These two parameters are correlated with other factors governing the physical process. These correlations would be useful in modeling mass transfer into matrix during solvent flow in fracture.

1. Introduction

The target oil in naturally fractured reservoirs (NFRs) exists in rock matrix. During the injection of tertiary recovery materials that are miscible with matrix oil, i.e., hydrocarbon solvents, alcohols, CO_2, N_2, etc., fracture network creates the path for the injected solvent to bypass and leave the unswept oil zones in the matrix. Significant amount of oil can be recovered from this upswept bypassed zone by maximizing the subsequent crossflow or mass transfer between fracture and media. Likewise, when greenhouse gases (CO_2, pure or in the form of flue gas) is injected into NFRs, the matrix part could be a proper storage environment and the transfer of the injected gas to matrix needs to be well understood for the determination of the process efficiency. The same process is encountered in the transportation of contaminants and waste material in NFRs.

In general four factors contribute to crossflow/mass transfer: (a) pressure, (b) gravity, (3) dispersion/diffusion, and (d) capillary drive. When the bypassed fluid and displacement fluids are first-contact miscible (FCM), there is no capillary crossflow. When the fluids are multi-contact miscible (MCM) or immiscible, there could be a certain degree of capillary-driven crossflow. Burger et al. [1,2] found that capillary-driven crossflow does not contribute significantly to mass transfer in near-miscible hydrocarbon floods. The other three forces play a critical role in the mass transfer between matrix and fracture and need to be well understood in terms of the effective parameters and efficiency of the process.

Previously we had performed experiments to clarify the effective parameters on the mass transfer during solvent injection into fractured systems [3]. In this study, the critical rate was defined as the maximum rate beyond which no change in the ratio of matrix recovery to injected solvent is obtained by increasing rate. As the injection rate is increased, the injected fluid flowing in the fracture would yield an early breakthrough without spending enough time to contact with the matrix. Hence, increasing rates may result in a faster recovery but higher amount of solvent is needed due to weaker mass transfer interaction to cause oil production from matrix. This results in an inefficient use of solvent. Therefore, slower rates are desirable for a better interaction and stronger mass transfer yielding higher matrix oil recovery to solvent injected ratio. This, however, reduces the recovery time. Thus, the definition of critical rate is an important issue and the rate depends on rock and fluid characteristics. The concept of critical velocity was first intro-

* Corresponding author.
E-mail address: tayfun@ualberta.ca (T. Babadagli).

1385-8947/$ – see front matter © 2008 Elsevier B.V. All rights reserved.
doi:10.1016/j.cej.2008.05.032

Nomenclature

A	total area for the core (m^2)
$2b$	fracture aperture (m)
CF	concentration in fracture, fraction
CM	concentration in matrix, fraction
D_{eff}	effective diffusion coefficient (m^2/s)
D_e^M	effective diffusion coefficient in matrix for matrix–fracture system (m^2/s)
D_L	effective dispersion coefficient in fracture (m^2/s)
D_m	mutual diffusion coefficient (m^2/s)
D_{mech}	mechanical dispersion coefficient (m^2/s)
g	gravitational force (m/s^2)
K_V	mass transfer rate constant (s^{-1})
N	flux
P	pressure (N/m^2)
Pe	Peclet number
Q	amount imbibed (m^3)
Q_S	source term
r	half fracture spacing (m)
S	saturation, fraction
t	time (s)
V	average fluid velocity in the fracture (m/s)
W_{factor}	wettability factor
x	coordinate direction along the fracture (m)
y	coordinate direction normal to the fracture (m)

Greek letters

κ	permeability (m^2)
ρ_f	density (kg/m^3)
μ	viscosity (kg/m s)

Subscripts

C	capillary
F	fracture
h	hydraulic
K	kerosene
m	mass transfer
M	matrix
R	reaction
S	surface
W	water
1	solvent
2	solute

duced by Thompson and Mungan [4]. They compared displacement velocity to critical velocity (V_C) and showed its effect on recovery efficiency. Firoozabadi and Markeset [5] showed that the capillary pressure contrast between matrix and fracture could be the major driving force. Further, they studied the effect of matrix/fracture configuration and fracture aperture on first-contact miscible efficiency.

Advanced visualization studies were also conducted to understand the physics of matrix–fracture interaction. Part [6] studied the formation of drying patterns assuming only capillary forces and neglecting viscous effects. It was the first attempt to theoretically characterize drying patterns in porous media as well. Computational [7,8] and experimental [9,10] studies on the interaction of matrix and fracture for different types of fluids were also reported.

The diffusion process and correlations of the capillary pressure with variation of interfacial tension were also investigated [11–13]. Morel et al. [11] performed diffusion experiments with chalk and studied the effect of initial gas saturation. The diffusion-stripping process in fractured media was well described by Saidi [14]. Recently, there has been success in determining diffusion coefficients between two miscible fluid systems [15–18] but the process is totally different within the fractured porous media, affected by many parameters such as matrix properties, condition at the boundaries, fracture geometry and flow conditions.

The presence of water affects the pore-scale distribution of hydrocarbon phases [19,20]. Connectivity and tortuosity of the pore structure influences the effective diffusivity and the relative permeability of each hydrocarbon phase. Hence the mass transfer and bypassing are affected. Le Romancer et al. [10] examined the effect of water saturation (<30%) on mass transfer in the matrix blocks of a fractured reservoir. As the water saturation increases, the liquid-hydrocarbon-phase area available for diffusion and the gas/liquid interfacial area decrease, and mass transfer decreases. At high water saturations, islands of oil will be isolated by water, effectively reducing mass transfer further. They concluded that water saturation has no effect during nitrogen injection because of a strong capillary crossflow. Wylie and Mohanty [21] further investigated the effects of water saturation on mass transfer from bypassed region and bypassing during miscible/near-miscible gas injection. They used 1D model and calculated effective diffusion coefficient.

The orientation of the bypassed region with respect to gravity and enrichment of the solvents affect the mass transfer rate. The mass transfer was least for the vertically up orientation (against gravity), intermediate for the vertically down, and highest for the horizontal orientation for the experiments [2]. Burger et al. [2] also concluded in his analysis that in vertical orientation gravity does not induce the flow of oil to the outlet face; therefore the recovery is primarily the result of diffusion. The oil-phase diffusivity is the controlling parameter in vertical mass transfer experiments.

Comings and Sherwood [22] modeled the process considering moisture moment by capillary in drying granular materials. But determining mass transfer coefficients during flow in fracture is more complex process due to the involvement of injection rate effect and fracture properties. In most of the available commercial simulators, the mass transfer is assumed to proceed by diffusion within single phase. Recent studies from Jamshidnezhad et al. [23] considered mass transfer between the same phases in the fracture and porous medium. In their work displacement was considered as one-dimensional and a few experiments were compared with the simulation results.

As seen, the miscible interaction process between matrix and fracture in naturally fractured subsurface reservoir has been studied for different purposes. The previous efforts were made usually to understand the physics of the interaction process through experimental studies. Limited number of studies focused on the numerical modeling usually without enough experimental support. Deriving correlations using dimensionless numbers to define matrix–fracture interaction terms is a critical task and that requires a combination of experimental and simulation work. Though much effort was devoted in defining the immiscible matrix–fracture interaction through dimensionless terms, less attention has been given to modeling miscible interaction, especially using controllable parameters such as injection rate and fluid characteristics. Also in simulation of the matrix–fracture fracture miscible interaction processes, 2-D or 3-D models have to be considered due to transverse mass transfer to and from the fracture and longitudinal diffusion/dispersion within the matrix and fracture individually. The understanding of the qualitative nature of the physics behind the matrix–fracture interaction process and quantitative representation of the controlling transfer parameters are the objectives of this paper and this was achieved through a series of experimental and numerical simulation works.

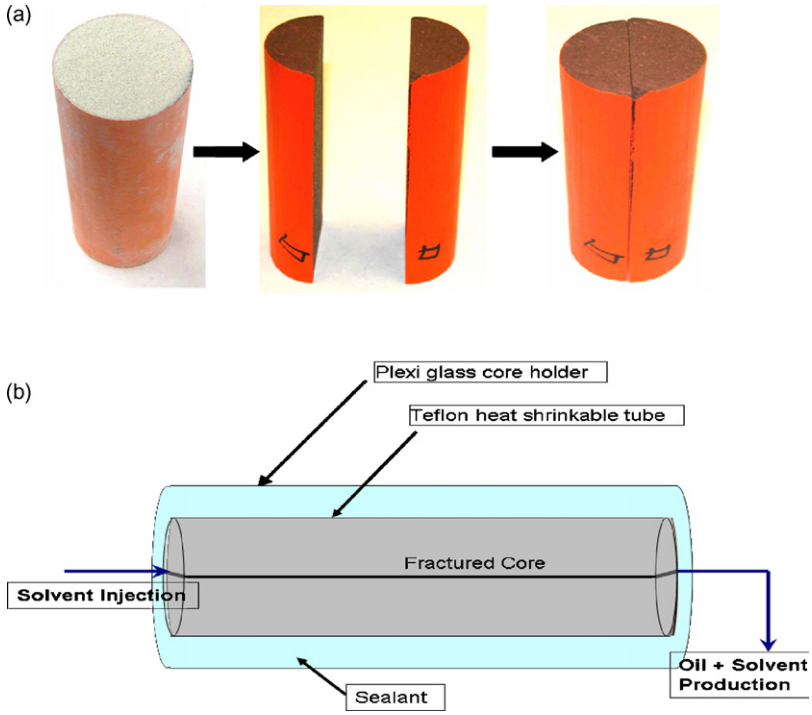

Fig. 1. (a) Core cutting and fracture preparation and (b) core holder design.

2. Experimental study

Experiments were performed to study and analyze the process of diffusion and dispersion during flow of solvent into the fracture adjacent to the oil saturated matrix qualitatively with change in length, solute type (hence the viscosity and density) and aging time with oil in the fractured porous media. These parameters affect the various forces, viscous and diffusion in particular, and alter the amount of oil produced and solvent diffused into the matrix with amount of solvent injected over the period of solvent injection process. Experimental observations will be useful in comparing and matching the results from the numerical simulations. Experimental analysis coupled with the numerical modeling will also be used to define and formulate critical parameters controlling the matrix–fracture interaction/transfer, which are not practically obtainable through direct experimental measurements or computations. To simplify the understanding of diffusion drive mechanism, we used FCM case and neglected capillary-driven crossflow. All the experiments were performed at room temperature and pressure to nullify the crossflow/mass transfer due to pressure drive.

2.1. Procedure

Cylindrical plugs were cut from 20 in. long cylindrical rods of Berea sandstone (k = 500 md; ϕ = 0.21) and Indiana limestone (k = 15 md; ϕ = 0.11) to 6 in. in length and 2 in. in diameter. Then, the samples were fully saturated with different solute under constant vacuum for 48 h using a vacuum pump. The saturated cores were cut into two pieces through the center in the direction of longitudinal axis for the purpose of creating a fracture. These pieces were held together using heat-shrinkable rubber sleeves.

The fractured core was then placed into Plexiglas holder and the annular space was filled with silicon to ensure no flow to the annulus between the core and core holder. The solvent was injected at constant rate from the center of the core and production line was placed at the center of other end. Injection and production were maintained only through the fracture while the flow into matrix was only through diffusion/mass transfer.

Flow through fractures was considered in several studies. There are three common ways of injection: (a) injection through matrix and production through matrix, while the fracture was located in the middle of the two matrix blocks; (b) injection through fracture and produce through fracture, while there is only one (or two) matrix block adjacent to fracture; (c) injection through circular annular acting as a fracture. In our experiments, we applied the injection scheme as defined in option (b) considering the fact that the flow will be controlled by high permeability fractures.

Some experiments were also performed with aged samples. In those cases cores were aged for a period of 1 month. Effect of solute viscosity and density were analyzed using different solute types (mineral oil, heavy-mineral oil, and kerosene).

The samples collected at the production end were analyzed using refractometer. Using the calibration curve from the known percentage of mixture, refractive index (RI) values were converted to obtain relative proportions in the production mixture. All the experiments were performed at room temperature.

Core preparation and experimental set-up are shown in Figs. 1 and 2, respectively. The properties of fluids used are given in Table 1. Detailed outline of experiments performed is listed in Table 2.

Table 1
Properties of solute and solvent used in the study

Chemical name	Density (g/cm^3)	Viscosity (cP)	Refraction index (RI)
Solvent			
Heptane	0.69	0.410	1.3891
Solute			
Mineral oil (MO)	0.83	33.5	1.469
High viscosity mineral oil (HO)	0.85	150	1.469
Kerosene	0.81	2.1	1.475

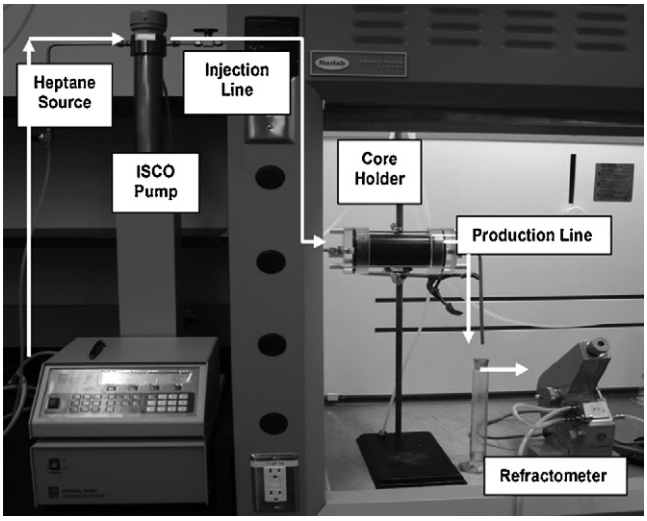

Fig. 2. Experimental set-up (adapted from previous study [3]).

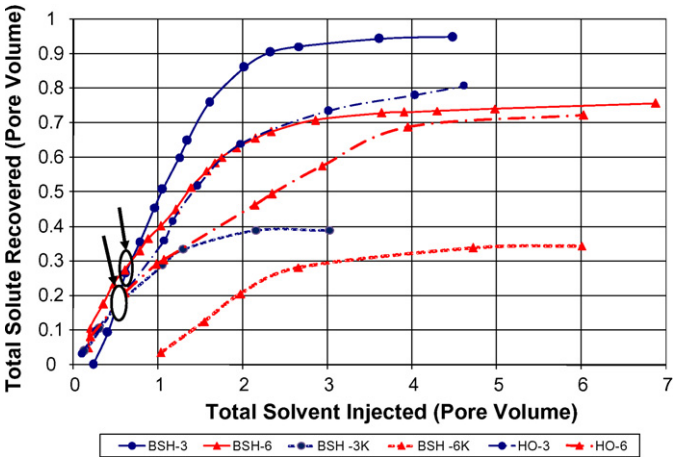

Fig. 3. Solute recoveries during solvent diffusion for different oil types.

3. Experimental observations

We used the plot of total solvent injection (as pore volume) vs. total oil (solute) recovered (as pore volume) to represent the results. The recovery of solute (oil) in *y*-axis corresponds to solvent concentration in the system. Because our main target was oil recovery in this particular study, we preferred to use solute recovered in *y*-axis rather than solvent concentration.

The diffusion dominant displacement front progresses slower when injecting solvent at a lower rate for all three solutes (oils) (Fig. 3). Although the solute recovery rates are slower compared to that of higher rate solvent injection, the final recoveries are higher for the lower rates. It was observed that the initial phase of the recovery curves are dominated by displacement or viscous forces and the diffusion comes into picture at later stage. Such phenomena can be detected at the point when recovery curve of BHS-3 overpasses that of BHS-6 as marked by an arrow in Fig. 3.

Different solute types, i.e. different densities and viscosities, may take part in the diffusion process between matrix and fracture. Some experiments were conducted to elaborate the range of viscosity and density of solute used. We used high viscosity mineral oil and kerosene for this purpose. Though the ultimate recoveries are lower for heptane diffusing into high viscosity mineral oil saturated sandstone, the crossover of lower rate injection case (HO-3) to higher rate injection case (HO-6) was evident (Fig. 3). Interestingly, it occurred after certain amount of pore volume solvent injected (or time). In case of kerosene, we were not able to capture this point. It possibly occurred either at very early stage of the process or did not ever happen. The lower-rate-diffusive-transfer dominates the solute production throughout the process. Based on these observations, one can conclude that density difference controls the process rather than the viscosity difference.

In contrast to the horizontal case where the effect of different flow rates was significant on ultimate recovery, the ultimate recoveries were similar during solvent diffusion at different rates in the vertically oriented sandstone (Fig. 4). However, solute recovery trends were in agreement with those of horizontal cases. It is worth noting that the BV-3 case overpasses the BV-6 case at around 40% of solute production. This turning point is higher than the point where BHS-3 overpasses the BHS-6. The total amounts of solute produced were also higher with almost similar amount of solvent required to reach the plateau of ultimate recovery, which makes a strong point of gravity influence.

Table 2
Details of experiments performed

Case	Core type	Angle (°)	Solute type	Flow rate (ml/h)	Matrix length (in.)	Aged
BSH-3	Sandstone	0	MO	3	6	No
BSH-6	Sandstone	0	MO	6	6	No
BSH-9	Sandstone	0	MO	9	6	No
BHA-3	Sandstone	0	MO	3	6	Yes
BHA-4.5	Sandstone	0	MO	4.5	6	Yes
BHA-6	Sandstone	0	MO	6	6	Yes
BHA-9	Sandstone	0	MO	9	6	Yes
BSK-3K	Sandstone	0	Kerosene	3	6	No
BSK-6K	Sandstone	0	Kerosene	6	6	No
BSV-3	Sandstone	90	MO	3	6	No
BSV-6	Sandstone	90	MO	6	6	No
HO-3	Sandstone	0	HO	3	6	No
HO-6	Sandstone	0	HO	6	6	No
HO-3 (3 in.)	Sandstone	0	HO	3	3	No
HO-6 (3 in.)	Sandstone	0	HO	6	3	No
HOA-3	Sandstone	0	HO	3	6	Yes
HOA-6	Sandstone	0	HO	6	6	Yes
ILH-3	Limestone	0	MO	3	6	No
ILH-6	Limestone	0	MO	6	6	No

H: horizontal; V: vertical; A: aged over period of 1 month; MO: mineral oil; HO: high viscosity oil.

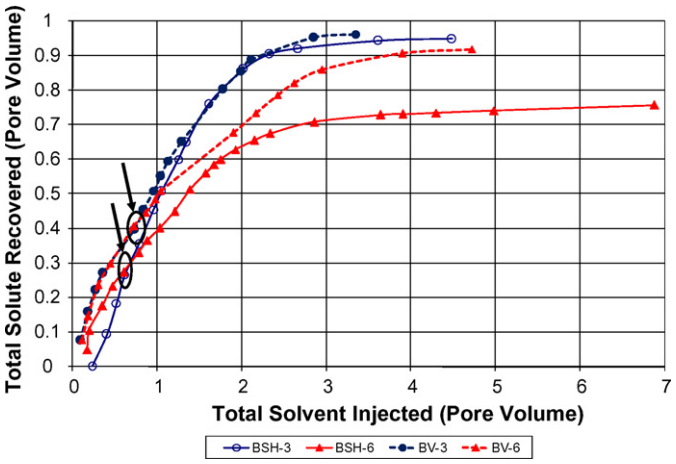

Fig. 4. Solute recoveries during solvent diffusion for horizontal and vertical cases.

The role of porosity and permeability was proved to be significant when similar injection and experimental conditions were applied for mineral oil saturated Berea sandstone and Indiana limestone (Fig. 5). The ultimate recovery from the limestone sample is almost half of the recovery observed in the sandstone cores. The trend was very much alike of sandstones where slower rate process overpasses the higher rate process at the same point of recovery. Noticeably this transition took place at nearly 35% oil production, just a bit higher than that of horizontal and vertical sandstone cases (30%). This point comes much later stage of time compared to that in sandstone, meaning that the poor porosity and permeability of the medium yield less efficient process.

Core aging affects the recovery trends. The recovery rate of mineral oil is slower and the ultimate recovery is lower for the aged Berea sandstones compared to those of non-aged samples. Fig. 6 points out the influence of aging on miscible flood efficiency. The comparison of such effect on recovery curves is illustrated using the cases of 3 ml/h and 6 ml/h flow rates for non-aged mineral oil saturated Berea sandstones and aged one (for a period of 1 month). No significant difference in terms of ultimate recovery was observed between aged and non-aged samples for heavy-mineral oil (Fig. 7). The amount of pore volume injected for obtaining ultimate recovery was also found unchanged with marginal difference compared to that of non-aged-viscous-oil-sandstone cases.

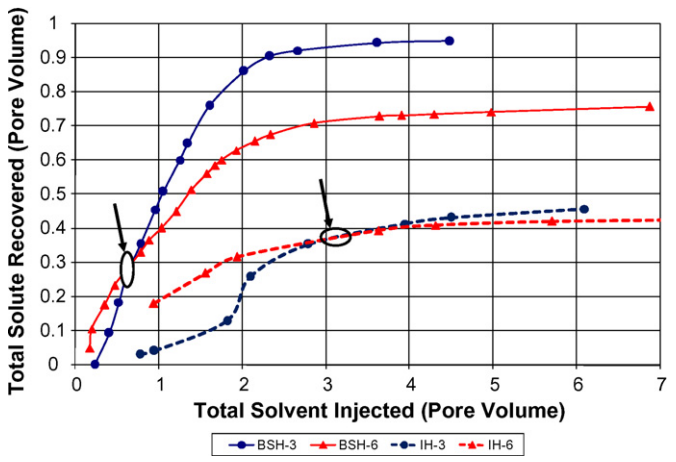

Fig. 5. Solute recoveries during solvent diffusion comparing Berea sandstone and Indiana limestone cores.

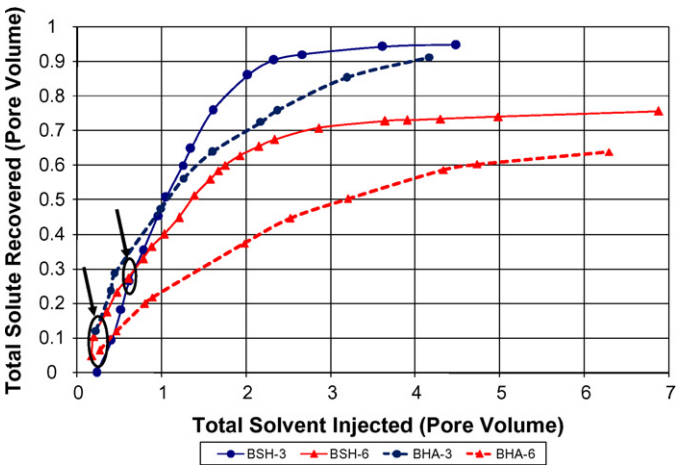

Fig. 6. Comparison of the solute recoveries during solvent diffusion for the aged and non-aged samples.

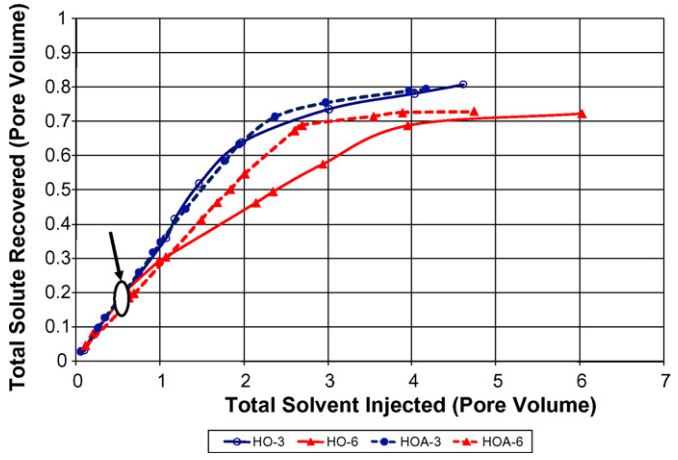

Fig. 7. Solute recoveries during solvent diffusion from high viscosity mineral oil aged and non-aged core samples.

When the size of the core was changed from 6 in. to 3 in. (Fig. 8), no significant effect was observed between the ultimate recoveries of the flow rate of 3 ml/h and 6 ml/h cases. But, more solvent needs to be injected to reach the same ultimate recovery in case of shorter

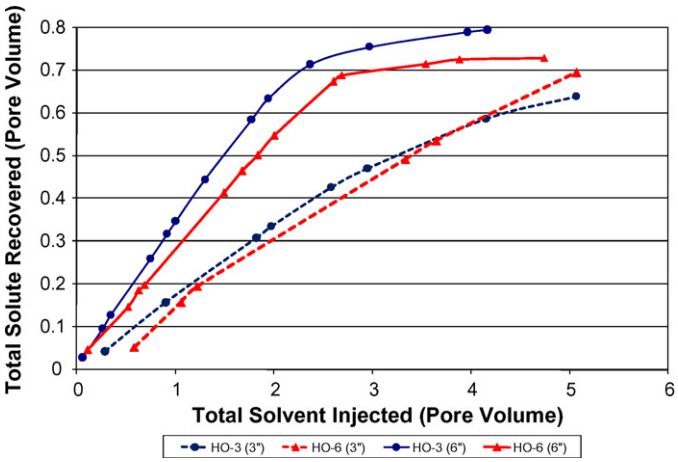

Fig. 8. Solute recoveries during solvent diffusion comparing 3 in. and 6 in. longer samples.

samples, implying that the recovery rate is lower. Solvent does not have enough time to contact with the rock matrix to diffuse into the matrix to sweep out the solute before it breaks through for the shorter samples. Hence, the length of the matrix size in determining the efficient transfer conditions is also important.

4. Modeling of fracture–matrix transfer process

Fracture–matrix transfer process was modeled numerically and presented in the form of dimensionless groups to analyze the effects of different parameters quantitatively. The process experimentally analyzed in the previous section was simulated using finite element modeling with the governing advection–convection equations and the Darcy equation. Only parameters other than those unavailable from the laboratory scale experiments are diffusion/dispersion coefficients and mass transfer coefficients in the matrix as well as in the fracture. These parameters were obtained through matching the numerical modeling results to their experimental equivalents and then they were correlated to fluid–rock properties and flow velocity.

4.1. Analogy between monolith catalysts (reactor) and matrix–fracture systems

Monolithic catalysts have gained recent interest for reducing pollution [24] due to simultaneous advantages of very low pressure drop, short diffusion resistance, excellent mass transfer and high surface to volume ratio. They are also widely used in selective catalytic reduction of NO_x, hydrogenations of liquid phase, power generation using gas turbines [25,26].

Monolithic catalysts/reactors (Fig. 9) consist of a matrix of uniformly aligned parallel channels. The diameter of the channel ranges from 0.5 mm to 10 mm and length can be up to 1 m long. These channels are fabricated on either ceramic or metallic supports called substrates. On the walls of the channels a catalytic active layer (a porous layer), 10–200 μm thick, can be applied. It is commonly called as *washcoat*. The flow is laminar in monolithic reactor for most of the applications with the Reynolds number typically in the range 10–1000. The reactants in the fluid phase are transported to the surface of the catalyst by convection and from the surface of the catalyst to the active sites of the catalyst by diffusion. The reactants react on the active catalysts sites which results in release or absorption of heat. The presence of catalytic reactions at the wall of the channel acts as a source or sink, which imposes temperature or concentration gradients in the radial directions.

The magnitude of radial gradients depends on the relative rates of heat and mass transfer and chemical reaction. There are two important types of potential mass transfer limitation in these reactors. The first is diffusion limitation in the washcoat owing to fast reaction. The rate of reaction is controlled by the intrinsic kinetics

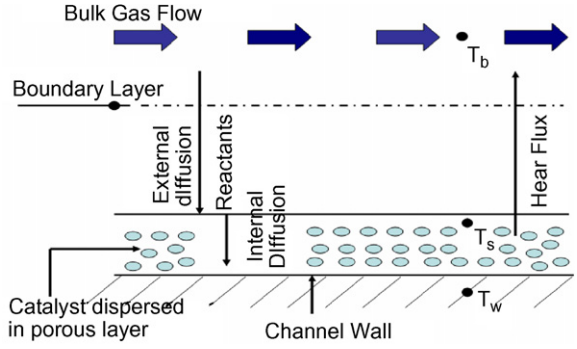

Fig. 9. Diffusion and flux behavior in monoliths.

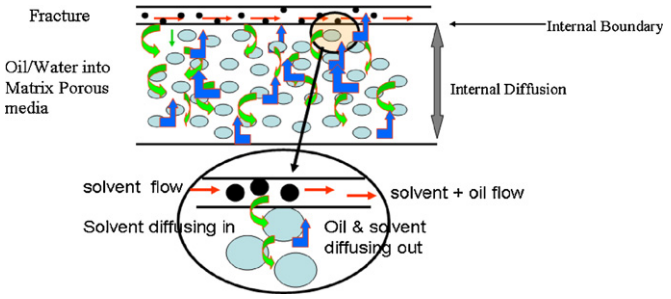

Fig. 10. Diffusion and flux in matrix–fracture system.

only and the reactor is said to be in kinetically controlled regime. If the rate of diffusion is lower than the intrinsic rate of reaction, the bulk and surface conditions are different. In the extreme case, the catalyst concentration at the surface may go zero and the rate is controlled solely by the rate of mass transfer.

The monolith reactors system (Fig. 9) is analogous to the matrix–fracture system in subsurface reservoirs as depicted in Fig. 10. The network of fracture channels run through less permeable porous media than fractures. Porous media can be visualized as porous washcoat. Injected solvent passes through fractures transferring to matrix interface through diffusion and convection. Within the matrix pores, solvent is transported through diffusion. For simplification, the whole network of channels is represented by a single channel with assumption of equivalent passages with no interaction. The same assumption applies while simulating the matrix–fracture system. The only difference is the size of porous media. Unlike the monolith reactor the size of porous media is considerably large in the fractured reservoirs. This may cause higher concentration or temperature gradients in the transverse directions, which is normal to the flow direction and hence the Sherwood numbers becomes remarkably higher than that exists into typical monolith catalyst. The physics of the process, however, is very much similar in both cases.

The mass or heat transfer within a single matrix can be described by two inherently coupled processes: external transfer from the bulk to the matrix and internal transfer inside the porous matrix. Hence, the steady-state behavior of a single matrix can be mathematically described by convection–diffusion equation in the fluid phase coupled with the diffusion–reaction equation within the porous media involving more than one spatial dimension similar to the single monolith channel reactor.

The shape of the washcoat geometry has large influence on the final conversion of reactants and mass transfer rate because of their small size (μm scale). While the matrix assumed here is of significantly larger size (cm scale) and considered rectangular shape. The effect of matrix shape is not the scope of this research and has to be focused separately.

4.2. Mathematical model formulation

The assumptions in the derivation of the equations are as follows:

- All fractures of the system are equivalent with uniform flow distribution and represent the network of fractures by a single straight channel.
- The oil is assumed to be dispersed uniformly within the porous matrix.
- In this analysis, we do not impose any restriction on the geometric shape of the fracture, except that the cross section of the fracture is invariant with the axial position.

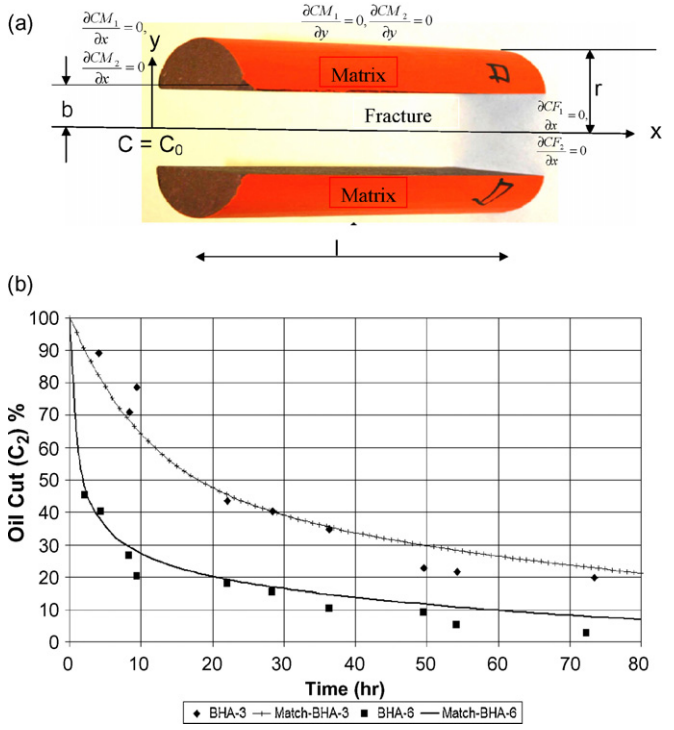

Fig. 11. (a) Geometrical representation of matrix–fracture system used in this study (not to scale). (b) Simulation match with the experimental results of solute (mineral oil) concentration (C_2) change for two different rates on aged Berea sandstone cores.

- The flow is laminar and fully developed.
- The aspect ratio of the channel is assumed to be small; that is, the hydraulic diameter is much smaller than the length of the fracture (which is true for most of the practical applications). This assumption justifies the use of fully developed velocity profile within the channel and also leads to the simplification of negligible axial diffusion in both fluid phase and matrix compared to the convective transport rate.
- The flow in the fracture is assumed isothermal.
- Solvent flows only through fractures; there is no flow in the matrix surrounding fracture.
- The variations of physical properties (such as density, viscosity, diffusivities, and so on) and velocity with temperature and compositions are neglected.

Fig. 11(a) represents the matrix–fracture system (length = l and radius = $2r$) with inlet, outlet as well as the boundary conditions. The pore space of the matrix is initially filled with a displaced fluid ($C_M = 1$) and is flooded with a displacing fluid ($C_F = 1$) from one side $x = 0$ at the center, where fracture (half aperture = b) is located. The x-axis is the principle flow direction, while the y-axis is the direction perpendicular to the flow. The displacing fluid (solvent) flows/injected at constant rate through fracture at the inlet $x = 0$; there is no flow in the matrix surrounding fracture.

The diffusion–convection equations for fracture and matrix are defined as follows:

Domain 1—fracture

$$\frac{\partial \mathrm{CF}_1}{\partial t} - D_\mathrm{L}\frac{\partial^2 \mathrm{CF}_1}{\partial x^2} - D_\mathrm{L}\frac{\partial^2 \mathrm{CF}_1}{\partial y^2} = -K_\mathrm{V}(\mathrm{CF}_1 - \mathrm{CM}_1) - u_\mathrm{F}\frac{\partial \mathrm{CF}_1}{\partial x} \quad (1)$$

$$\frac{\partial \mathrm{CF}_2}{\partial t} - D_\mathrm{L}\frac{\partial^2 \mathrm{CF}_2}{\partial x^2} - D_\mathrm{L}\frac{\partial^2 \mathrm{CF}_2}{\partial y^2} = -K_\mathrm{V}(\mathrm{CF}_2 - \mathrm{CM}_2) - u_\mathrm{F}\frac{\partial \mathrm{CF}_2}{\partial x} \quad (2)$$

Domain 2—matrix

$$\frac{\partial \mathrm{CM}_1}{\partial t} - D_\mathrm{e}^\mathrm{M}\frac{\partial^2 \mathrm{CM}_1}{\partial x^2} - D_\mathrm{e}^\mathrm{M}\frac{\partial^2 \mathrm{CM}_1}{\partial y^2} = K_\mathrm{V}(\mathrm{CF}_1 - \mathrm{CM}_1) \quad (3)$$

$$\frac{\partial \mathrm{CM}_2}{\partial t} - D_\mathrm{e}^\mathrm{M}\frac{\partial^2 \mathrm{CM}_2}{\partial x^2} - D_\mathrm{e}^\mathrm{M}\frac{\partial^2 \mathrm{CM}_2}{\partial y^2} = K_\mathrm{V}(\mathrm{CF}_2 - \mathrm{CM}_2) \quad (4)$$

Initial conditions:

$$\mathrm{CF}_1(x, y, 0) = 0; \quad \mathrm{CM}_1(x, y, 0) = 0; \quad \mathrm{CF}_2(x, y, 0) = 1;$$
$$\mathrm{CM}_2(x, y, 0) = 1; \quad \mathrm{CF}_1(0, t) = \mathrm{CF}_0 \quad (5)$$

Boundary conditions:

$$\left.\frac{\partial \mathrm{CM}_1}{\partial y}\right|_{(x,r,t)} = 0; \quad \left.\frac{\partial \mathrm{CM}_2}{\partial y}\right|_{(x,r,t)} = 0 \quad (6)$$

$$\left.\frac{\partial \mathrm{CF}_1}{\partial x}\right|_{(\infty,t)} = 0; \quad \left.\frac{\partial \mathrm{CF}_2}{\partial x}\right|_{(\infty,t)} = 0 \quad (7)$$

$$D_\mathrm{L}\frac{\partial \mathrm{CF}_1}{\partial y} = -D_\mathrm{e}^\mathrm{M}\frac{\partial \mathrm{CM}_1}{\partial y}; \quad D_\mathrm{L}\frac{\partial \mathrm{CF}_2}{\partial y} = -D_\mathrm{e}^\mathrm{M}\frac{\partial \mathrm{CM}_2}{\partial y} \quad \text{at } t = t \ \forall x, b \quad (8)$$

We used finite element method (FEM) to solve the partial differential equation using COMSOL multiphysic [27]. The finite element method approximates a PDE problem with a problem that has a finite number of unknown parameters. The advantages of FEM are the ease of handling complex geometries, straightforward implementation of non-uniform meshes, and the simple incorporation of flux boundary conditions. Galerkin method is used to solve the partial differential equations.

The system is described by Eqs. (1)–(4), with the initial and boundary conditions given in Eqs. (5)–(8). The grid size in the fracture is maintained constant while the grid size varies in the matrix. Transient analysis with time dependent solver (direct (Spooles) linear system solver) is used. The Spooles linear solver makes use of the symmetry in the diffusion equation and saves memory. A second order in space and time discretization is adopted with an implicit time stepping to achieve accurate results. The temporal simulations with increasing time steps starting with a small time step are made. The simulation results were compared with the results of experimental performed earlier. From the numeric simulations, values of K_V and D_e^M were obtained. In fact, they are the two critical parameters controlling the matrix–fracture interaction and functions of several different flow, fluids, fracture, and matrix properties. All other parameters were experimentally available, measurable, or computable. Comparison of simulated and experimental results is shown for two different cases in Fig. 11.

Note that the early time behavior (initial straight line portion before the curvature) was observed to be dominated by the K_V and the later part by the D_e^M. The early time behavior is not controlled by the D_e^M. Therefore, the solution of the equation is assumed to be unique.

4.3. Dispersion and diffusion

Miscible recovery is the process in which solvent and solute are completely miscible with each other either first-contact or multicontact. The concentration changes from that of solute to solvent inside the porous media till the equilibrium reaches. Due to miscible nature of the process (no interfacial tension), in such process there is no existence of capillary or inter-phase forces. Theoretically complete sweep is possible and 100% recovery of solute can be

achieved at the equilibrium stage. The driving forces are molecular diffusion and convection.

During the flow through porous media, the additional mixing caused by uneven flow or concentration gradient is called dispersion. It results from the different paths and speeds and the consequent range of transit times available to tracer particles convected across a permeable medium. Dispersive mixing is a resultant of molecular diffusion and mechanical dispersion. Perkins and Johnston [28] have provided an analysis of the dispersion phenomena and correlations for two types of dispersion: (1) longitudinal direction, and (2) transverse to the direction of gross fluid movement. Both, having different magnitude, have to be considered separately. Dispersive mixing plays important role in determining how much solvent will dissolve/mix with solute to promote miscibility. Molecular diffusion will cause mixing along the interface. The net result will be a mixed zone growing at a more rapid rate than would obtain from diffusion alone. Diffusion is a special case of dispersion and a result of concentration gradient, with or without the presence of the velocity field [29,30].

Gillham and Cerry [31] defined the hydrodynamic dispersion coefficient as the sum of coefficient of mechanical dispersion (D_{mech}) and the effective diffusion coefficient in the porous media (D_{eff}). The hydrodynamic dispersion coefficient is also referred as dispersion–diffusion coefficient (D_L):

$$D_L = D_{mech} + D_{eff} \tag{9}$$

The mechanical dispersion is proportional to the average linearized pore-water velocity (V) and the dispersivity (α) [32,33]. The effective diffusion coefficient is related to diffusion coefficient in free solution and tortuosity.

Taylor [34] showed that in case of substantial diffusion perpendicular to the average fluid velocity, the dispersion coefficient in the tube would be proportional to the square of the average fluid velocity. Later, Horne and Rodriguez [35] concluded that in the diffusion dominated system, the dispersion coefficient in the single, straight, parallel plate fracture will be proportional to the square of the fluid velocity. Keller et al. [36] showed that dispersion coefficient and velocity have linear relationship, where $D_L \propto V$. Bear [32] suggested that the relation between dispersion coefficient and the average fluid velocity would be $D_L = \alpha V^n$. The range of the n value is limited to $1.0 \le n \le 2.0$.

From the findings of Ippolite et al. [37] and Roux et al. [38], it is known that the dispersion coefficient in the variable aperture fracture is the sum of molecular diffusion, Taylor dispersion and microscopic dispersion.

The Peclet number Pe for the flow in fracture is defined as

$$Pe = \frac{Vb}{D_m} \tag{10}$$

where V is the average fluid velocity in the fracture, b is the fracture aperture and D_m is the molecular diffusion coefficient.

Dronfield and Silliman [39] conducted transport experiments in sand-roughened analog fracture and came up with a relation as $D_L \propto Pe^{1.4}$. He also suggested that the power term to be 2 for parallel plate fracture and 1.3–1.4 for rough fractures. Detwiler et al. [40] studied the effect of Pe on D_L using experiments and numerical results. His investigations were in accordance with that of earlier from Ippolite et al. [37] and Roux et al. [38]. Molecular diffusion dominates within the regime of $Pe \ll 1$. The Taylor dispersion and microscopic dispersion are related to Pe. The Taylor dispersion is proportional to Pe^2 while microscopic dispersion is proportional to Pe. Detwiler et al. [40] showed quadratic relation from the result of Roux et al. [38] in the form of a first-order approximation of the total non-dimensional longitudinal dispersion coefficient:

$$\frac{D_L}{D_m} = \alpha_{Taylor}(Pe)^2 + \alpha_{macro}(Pe) + \tau \tag{11}$$

They further mentioned that for typical Pe ranges, τ (tortuosity for fracture) can be neglected.

The Taylor dispersion coefficient defined for parallel plate fracture is [34,41,42]:

$$D_{L,Taylor} = \frac{1}{210}\frac{V^2 b^2}{D_m} \tag{12}$$

$$\frac{D_{L,Taylor}}{D_m} = \frac{1}{210}\frac{V^2 b^2}{{D_m}^2} \tag{13}$$

$$D_{L,Taylor} = \frac{D_m}{210} \times (Pe)^2 \tag{14}$$

In our case, we assumed $D_L \propto Pe^{1.5}$, an average value of Taylor and microscopic dispersions, and used this calculated value for the dispersion coefficient in fracture. The value of D_m in our set of experiments will be the mutual diffusion coefficient of heptane and particular oil type. It is 3.2×10^{-9} m^2/s and 3×10^{-8} m^2/s for heptane–mineral oil and heptane–kerosene, respectively.

4.4. Mass transfer rate constant and effective diffusion into porous matrix

In simple terms, mass transfer is moving of fluid material from one point to another. For porous media it is the getting the material into and out of pores. Also for reactive process, the speed at which a chemical reaction proceeds, in terms of amount of product formed or amount of reactant consumed is also important. When there is no reaction, transfer rate is mostly due to diffusion and mixing. This transfer rate between two fluid pairs, solvent and solute, is presented by mass transfer rate constant (K_V). The increase of K_V indicates better mixing of solvent and solute, which results in faster approach to equilibrium conditions.

Fig. 12 clearly suggests that K_V is related to velocity, solvent–solute properties, and matrix properties as well as aging. Increase of velocity results into rapid circulation, enhanced mixing and better mass transfer. It is also evident that with the same type of cores and aging time, the increase in K_V is controlled mainly by the velocity (Fig. 12). As the velocity increases, the rate constant value increases and the values vary from each other with considerable margin.

Different amount of solute recoveries were observed when cores were aged for different periods of time after complete saturation

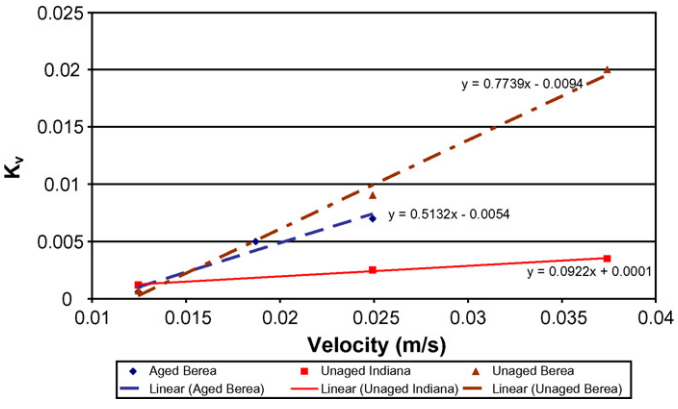

Fig. 12. Mass transfer rate constant with velocity. (For interpretation of the references to colour in this figure legend, the reader is referred to the web version of the article.)

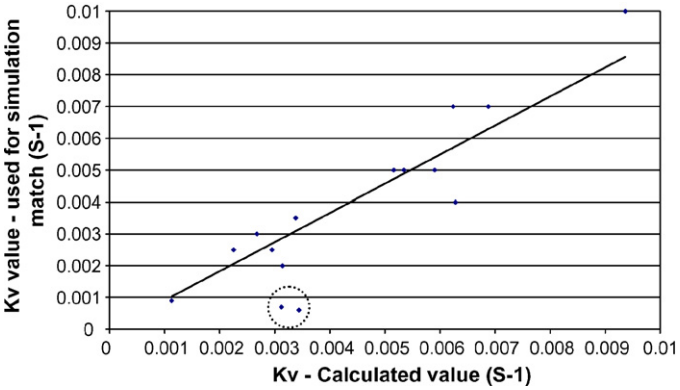

Fig. 13. Comparison of the K_V (s^{-1}) values obtained through the numerical simulation and the ones obtained from Eq. (17).

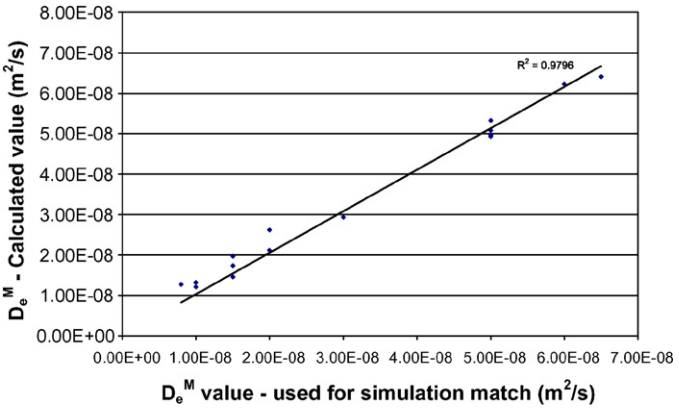

Fig. 14. Comparison of D_e^M values used for the simulation matches with the ones obtained from Eq. (18).

(Figs. 6 and 7). Although there is no water present in core samples, this can be interpreted as wettability change. To quantify the effect of aging time (or wettability change), we used spontaneous water imbibition data presented by Hatiboglu and Babadagli [43] and Trivedi and Babadagli [44] and on the same core and oil types based on Handy's approach [45].

$$Q_w^2 = \left(\frac{2P_C\kappa_w\phi A^2 S_w}{\mu_w}\right) t \tag{15}$$

The initial slop of the straight line from Q^2 against time were measured and normalized against the highest slope to obtain the P_C (known as effective capillary pressure) [44]. The changing slope reflects changing wettability caused by the aging as all other rock and fluid properties remained the same as observed by Trivedi and Babadagli [44].

The capillary pressures obtained from the experimental results of Refs. [43,44] were normalized based on the capillary pressure of kerosene and multiplied with viscosity ratio of solvent to solute to get wettability factor [44]. To incorporate the effect of solute viscosity, we defined the following dimensionless term (wettability factor, W_{factor}):

$$W_{factor} = \left(\frac{P_C}{P_{CK}}\right)\left(\frac{\mu_2}{\mu_1}\right) \tag{16}$$

P_C is obtained for each oil and rock type using Eq. (15) and P_{CK} is the P_C value for kerosene, which gives the highest slope due to its strong imbibition into matrix driven by its low viscosity.

To quantify the transfer rate constant for different wettability and porosity cores, it was represented as a function of velocity, wettability factor (W_{factor}), porosity of matrix, viscosity and density ratio of solute and solvent:

$$K_V = V(W_{factor})^{-0.15}(\phi)^{0.9}\left(\frac{\mu_2}{\mu_1}\right)^{0.06}\left(\frac{\rho_2}{\rho_1}\right) \tag{17}$$

Within porous media, the solute and solvent are transferred into and out of the pores by dispersion–diffusion mechanism. Since the solvent is injected into the fracture, there is no direct flow into the matrix porous media. Hence, we are not concerned with dispersion into the adjacent matrix. But there is an induced flow because of the flux transferred from the fracture at the interface and diffusion within the matrix. This complex process inside the porous media can be seen as an effect of dispersion into fracture and mass trans-

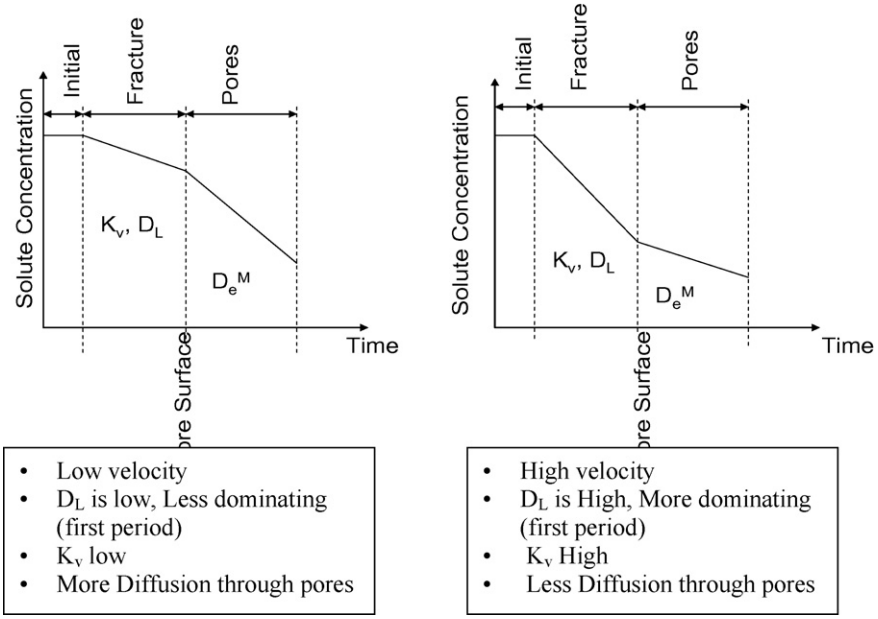

Fig. 15. Concentration–time curves for matrix–fracture transfer at low and high rates.

fer between two fluids, solvent and solute. Therefore, the resultant effective diffusion coefficient into the porous media is not only because of tortuosity but also because of mass transfer rate constant and dispersion occurring into fracture.

This effective diffusion coefficient into the matrix is represented as a function of solvent and solute properties, rock properties, mass transfer rate constant and the Taylor dispersion coefficient as follows:

$$D_e^M = \sqrt{D_{L,Taylor}\frac{(k/K_V)\phi(\mu_2/\mu_1)}{\rho_2/\rho_1}} \quad (18)$$

where k is the matrix permeability, K_V is the mass transfer rate constant, ϕ is the matrix porosity. The value of effective diffusion coefficient within the matrix (D_e^M) was one of the parameters tuned to obtain the match with experimental results of solvent concentration in the effluent. The effective matrix diffusion coefficient (D_e^M) calculated as shown above was in good agreement with that used during simulations (Fig. 14).

Note that the matrix size was not found critical in the correlations given in Eqs. (17) and (18). A good agreement was obtained for both shorter and longer samples as shown in Figs. 13 and 14. The only two points off line in Fig. 13 are for the low rate (3 ml/h) experiments. In those cases, the process is strongly controlled by the diffusion as the solvent has significantly more time to contact with matrix due to slow flow rate in the fracture. In other words, the effects of flow and diffusion in fracture are minimal.

In our process, mass transfer occurs in two different ways. One is in the fracture and it takes place between fluid mixtures until the oil in the fracture is exhausted. This process is controlled dominated by K_V and D_L. The second one is in the matrix pores and controls the remaining part of the process. This part is governed by K_V and D_e^M. This fact is well justified in the experimental results when the higher rate solute recovery curve dominates in the earlier period of time during which the essential solute fracture has been recovered. At later stages, dominated by D_e^M, the lower rate solute recovery curve overpasses the one with the higher rate suggesting the influence of pore diffusion. This process was schematically presented as the concentration–time curve in Fig. 15.

5. Conclusions

1. The experimental results indicated that the recovery through the fracture is dominated by the Peclet number (dispersion effect) and mass transfer rate constant (K_V). Hence, at the earlier stage of the production life (when the fracture oil recovery is effective) higher rate solvent injection should be preferred.
2. Considering overall effect and assuming the solute inside the matrix pores is larger in amount compared to that in the fracture, the effective diffusion coefficient (D_e^M) is the major controlling parameter and slower rate solvent injection with more retention time for effective diffusive flux to transfer from matrix yields better recovery.
3. The porous media aged over a period of time behaved different than that of non-aged one depending on the solute properties. The wettability factor presented here and further used in the study proved handy tool for inclusion of aging effect.
4. Length of the matrix being one of the important parameter because of the solvent breakthrough was noticed during experiments. Shorter cores, having less time for solvent to diffuse in transverse direction into porous matrix, showed lower solute recovery in a given time and rate compared to the longer ones.
5. We, however, did not observe significant effect of matrix size on the mass transfer rate constant (K_V) and effective diffusion coefficient in matrix (D_e^M).
6. The mass transfer rate and effective matrix diffusion coefficient were found to be linearly dependent on velocity and also affected by wettability as well as rock properties.
7. K_V and D_e^M, not available from any means of laboratory experiments, can be easily computed for miscible solvent processes in fractured porous media using the correlations provided here with fairly good amount of accuracy.

Acknowledgements

This study was partly funded by an NSERC Strategic Grant (No. G121210595) and FSIDA (University of Alberta, Fund for Support of International Development Activities) Grant (#04-14O). The funds for the equipment used in the experiments were obtained from the Canadian Foundation for Innovation (CFI, Project #7566) and the University of Alberta.

References

[1] J.E. Burger, K.K. Mohanty, Mass transfer from bypassed zones during gas injection, SPERE 12 (May (2)) (1997) 124.
[2] J.E. Burger, G. Springate, K.K. Mohanty, Experiments on bypassing during gas floods in heterogeneous porous media, SPERE 11 (May (2)) (1996) 109.
[3] J. Trivedi, T. Babadagli, Efficiency of miscible displacement in fractured porous media, in: Paper Presented at the SPE Western Regional/AAPG Pacific Section/GSA Cordilleran Section Joint Meeting, SPE 100411, Anchorage, Alaska, USA, May, 2006.
[4] J.L. Thompson, N. Mungan, A laboratory study of gravity drainage in fractured systems under miscible conditions, SPEJ 247 (June) (1969).
[5] A. Firoozabadi, T.I. Markeset, Miscible displacement in fractured porous media. Part I. Experiments, in: Paper Presented at the SPE/DOE 9th Symposium on Improved Oil Recovery, SPE 27743, Tulsa, OK, April, 1994.
[6] M. Part, Percolation model of drying under isothermal conditions in porous media, Int. J. Multiphase Flow 19 (1993) 693.
[7] S.N. Zakirov, A.N. Shandrygin, T.N. Segin, Miscible displacement of fluids within fractured porous reservoirs, in: Paper Presented at the 66th SPE Annual Technical Conference and Exhibition, SPE 22942, Dallas, TX, October, 1991.
[8] T.B. Jensen, M.P. Sharma, H.G. Harris, D.L. Whitman, Numerical investigations of steam and hot-water flooding in fractured porous media, in: Paper Presented at the SPE/DOE Eighth Symposium on Enhanced Oil Recovery, SPE 24172, Tulsa, OK, April, 1992.
[9] Hujun, Li, E. Putra, D.S. Schechter, R.B. Grigg, Experimental investigation of CO_2 gravity drainage in a fractured system, in: Paper Presented at the SPE Asia Pacific Oil & Gas Conference and Exhibition, SPE 64510, Brisbane, Australia, October, 2000.
[10] J.F. Le Romancer, D.F. Defives, G. Fernandes, Mechanism of oil recovery by gas diffusion in fractured reservoir in presence of water, in: Paper Presented at the SPE/DOE Ninth Symposium on Improved Oil Recovery, SPE 27746, Tulsa, OK, April, 1994.
[11] D.D. Morel, B. Bourbiaux, M. Latil, B. Thiebot, Diffusion effects in gas flooded light oil fractured reservoirs, SPE-Adv. Tech. Ser. 1 (2) (1993) 100–109.
[12] H. Hu, C.H. Whitson, Y. Ai, A study of recovery mechanisms in a nitrogen diffusion experiment, Unsolicited Paper Available in Society of Petroleum Engineers e-library, SPE 21893, 1991.
[13] J.F. Gabitto, Matrix–fracture mass transfer, in: Paper Presented at SPE/DOE Improved Oil Recovery Symposium, SPE 39702, Tulsa, OK, April, 1998.
[14] A.M. Saidi, Reservoir Engineering of Fractured Reservoir, Total Edition Press, 1987.
[15] C. Yang, Y. Gu, A new method of measuring solvent diffusivity in heavy oil by dynamic pendant drop shape analysis (DPDSA), SPEJ 11 (March (1)) (2006) 48.
[16] F. Civan, M.L. Rasmussen, Improved measurement of gas diffusivity for miscible gas flooding under nonequilibrium and equilibrium conditions, in: Paper Presented at SPE/DOE Improved Oil Recovery Symposium, SPE 75135, Tulsa, OK, April, 2002.
[17] M.R. Raizi, New method for experimental measurement of diffusion coefficients in reservoir fluids, J. Pet. Sci. Eng. 14 (May (3–4)) (1996) 235.
[18] A.K. Stubos, S. Poulou, Oil recovery potential from fractured reservoirs by mass transfer processes, in: Paper Presented at the SPE Annual Technical Conference and Exhibition, SPE 56415, Houston, TX, October, 1999.
[19] K.K. Pande, F.M. Orr, Jr., Analytical computation of breakthrough recovery for CO_2 floods in layered reservoirs, Unsolicited Paper Available in Society of Petroleum Engineers e-library, SPE 20177, 1990.
[20] K.K. Mohanty, S.J. Salter, Multiphase flow in porous media: II- pore-level modeling, in: SPE 11018, Paper Presented at the SPE Annual Technical Conference and Exhibition, New Orleans, September, 1982.
[21] P. Wylie, K.K. Mohanty, Effect of Water saturation on oil recovery by near-miscible gas injection, SPERE 12 (November (4)) (1997) 264.
[22] F.W. Comings, T.K. Sherwood, The drying of solids, moisture movement by capillarity in drying granular materials, Ind. Eng. Chem. 26 (1934) 1096.

[23] M. Jamshidnezhad, M. Montazer-Rahmati, V.A. Sajjadian, Theoretical and experimental investigations of miscible displacement in fractured porous media, Transp Porous Media 57 (October (1)) (2004) 59.
[24] A. Cybulski, J.A. Moulin, Structured Catalysis and Reactors, Marcel Dekker, New York, 1998.
[25] A. Cybulski, J.A. Moulin, Monoliths in Heterogeneous Catalysis, Catal. Rev. Sci. Eng. 36 (1994) 179.
[26] P. Forzatti, Present status and perspectives in de-NO_x SCR analysis, Appl. Catal. A: Gen. 222 (2001) 221.
[27] COMSOL, COMSOL Multiphysics, 3.2 ed., Stockholm, Sweden, 2006.
[28] T.K. Perkins, O.C. Johnston, A review of diffusion and dispersion in porous media, SPEJ 3 (4) (1963) 70, Trans. AIME 228 (1) (1963) 70.
[29] J. Bear, Dynamics of Fluids in Porous Media, Dover Publications Inc., New York, 1988.
[30] M. Sahimi, A.A. Heiba, B.D. Hughes, H.T. Davis, L.E. Scriven, Dispersion in flow through porous media, in: Paper Presented at the SPE Annual Technical Conference and Exhibition, SPE 10969, New Orleans, September, 1982.
[31] R. Gillham, J.A. Cerry, Contaminant migration in saturated unconsolidated geologic deposits, in: T.N. Narasimhan (Ed.), Recent Trends in Hydrogeology, Special Paper 189, Geological Society of America, pp. 31–62, 1982.
[32] J. Bear, Hydraulics of Groundwater, McGraw Hill, 1979.
[33] R.A. Freeze, J.A. Cherry, Groundwater, Prentice-Hall, Englewood Cliffs, NJ, 1979.
[34] G. Taylor, Dispersion of soluble matter in solvent flowing slowly through a tube, Proc. R. Soc. A 219 (1137) (1953) 186.
[35] R.N. Horne, F. Rodriguez, Dispersion in tracer flow in fractured geothermal systems, Geophys. Res. Lett. 10 (4) (1983) 289.
[36] A.A. Keller, P.V. Roberts, M.J. Martin, Effect of fracture aperture variations on the dispersion of solutes, Water Resour. Res. 35 (1) (1999) 55.
[37] I. Ippolito, G. Daccord, E.J. Hinch, J.P. Hulin, Echo tracer dispersion in model fractures with a rectangular geometry, J. Contam. Hydrol. 16 (May (1)) (1984) 87.
[38] S. Roux, F. Plouraboue, J.P. Hulin, Tracer dispersion in rough open cracks, Trans. Porous Media 32 (July (1)) (1998) 97.
[39] D.G. Dronfield, S.E. Silliman, Velocity dependence of dispersion for transport through a single fracture of variable roughness, Water Resour. Res. 29 (October (10)) (1993) 3477.
[40] R.L. Detwiler, H. Rajaram, R.J. Glass, Solute transport in variable-aperture fractures: an investigation of the relative importance of Taylor dispersion and macrodispersion, Water Resour. Res. 36 (July (7)) (2000) 1611.
[41] R. Aris, On dispersion of a solute in a fluid flowing through a tube, Proc. R. Soc. London A 235 (1200) (1956) 66.
[42] H.B. Fischer, E.J. List, R.C.Y. Koh, J. Imberger, N.H. Brooks, Mixing in Inland and Coastal Waters, Academic Press, San Diego, CA, 1979.
[43] C.U. Hatiboglu, T. Babadagli, Experimental analysis of primary and secondary oil recovery from matrix by counter-current diffusion and spontaneous imbibition, in: Paper Presented at the SPE Annual Technical Conference and Exhibition, SPE 90312, Houston, TX, September, 2004.
[44] J. Trivedi, T. Babadagli, Efficiency of diffusion controlled miscible displacement in fractured porous media, Transp. Porous Med. 71 (February (3)) (2008) 379.
[45] L. Handy, Determination of effective capillary pressure for porous media from imbibition data, AIME Trans. 219 (1960) 75.